Multibasin Dynamics in Off-Lattice Minimalist Protein Landscapes†

Yasuhiro Matsunaga,‡ Konstantin S. Kostov,§ and Tamiki Komatsuzaki*,‡

Nonlinear Science Laboratory, Department of Earth and Planetary Sciences, Faculty of Science, Kobe University, Nada, Kobe 657-8501, Japan, and Department of Chemistry, The University of Chicago, 5735 South Ellis Avenue, Chicago, Illinois 60637

Received: March 17, 2002

We analyze time series of potential energy fluctuations and principal components at several temperatures for two kinds of off-lattice 46-bead models that have two distinctive energy landscapes. The less-frustrated "funnel" energy landscape brings about stronger nonstationary behavior of the potential energy fluctuations at the folding temperature than the other, rather frustrated energy landscape at the collapse temperature with a significant $1/f^{\alpha}(\alpha \approx 1.5)$ noise structure and a significant deviation of the Allan variance from the law of large numbers. The principal components are analyzed by an embedding nonlinear time-series analysis. The fast fluctuations with small amplitudes of ∼70−80% of the principal components cause the time series to become almost "random" in only 100 simulation steps. However, the stochastic feature of the principal components tends to be suppressed through a wide range of degrees of freedom at the transition temperature.

I. Introduction

The questions What kinds of mechanisms carry a protein into a unique native state? and What is the best reaction coordinate to describe the dynamics of protein folding? have been one of the most intriguing subjects over the past decades.[1,2] Protein folding may be well interpreted as a normal Brownian process of a few collective coordinates on a thermodynamic potential such as the "funnel" landscape.[3−5] The diffusive nature may, however, depend on the choice of the viewpoint from which one might see the dynamical events. The fraction of native contacts Q is often taken as a reaction coordinate or global order parameter. However, it is not self-evident, as discussed by Karplus,[2] that Q is always appropriate to represent the progress of folding, and many different sets of contacts may yield the same value. There exists the nontrivial question, Are motions along this coordinate Q actually slow enough to average out any dynamical contribution of all the other degrees of freedom, resulting in an effective single, dominant free-energy barrier of folding? García and Hummer[6] showed how non-Brownian, strange kinetics[7] emerge in multibasin dynamics trajectories generated by all-atom molecular dynamics (MD) simulations of cytochrome c in aqueous solution at 300−550 K for at least 1.5 ns. They analyzed the mean square displacement (MSD) autocorrelation function in terms of molecule optimal dynamic coordinates (MODC). MODCs are collective coordinates derived by a linear transformation of the $3N$ Cartesian coordinates of the protein system (N = the number of atoms in the protein) that best represent the configurational protein fluctuations (in a least-squares sense). They found that the MSD along some slow MODCs manifestly exhibits non-Brownian dynamics between a temperature at which the protein is in the native state and a temperature above the melting point, where the hydrophobic effect is large and mostly enthalpic. In this temperature range, the MSD has a power-law time dependence with an exponent of nonunity (about 0.5 for times shorter than 100 ps and 1.75 for longer times). This indicates that protein motions are more suppressed and cover less configurational space than a normal Brownian process on a short time scale, but they become more enhanced as a faster, well-concerted motion on a long time scale. At a temperature where unfolding may occur in nanoseconds, normal Brownian dynamics seemingly emerges along the MODCs. Plotkin and Wolynes[8] studied, using an overdamped generalized Langevin formulation with Q as the reaction coordinate, how non-Markovian configurational diffusion enhances the folding rate over the Kramers rate in a certain T_f/T_g ($\simeq$1.6) regime (where T_f and T_g are, respectively, the folding and glass transition temperatures) and addressed how the inclusion of the other degrees of freedom into the reaction coordinate is essential for obtaining the optimal dividing surface for folding. Takano et al.[9] showed in a two-state-like helix−coil transition of a helical polypeptide that a $1/f$ noise structure of the potential energy fluctuations emerges at the transition temperature whereas away from that temperature the power α of $1/f^{\alpha}$ goes to zero, indicating a transition to a Markovian process. Nymeyer, García, and Onuchic[10] investigated, using an off-lattice 46-bead model that folds into a β-barrel native structure, how the energy landscape of the protein affects the folding kinetics. They found that the folding rate on a minimally frustrated funnel landscape exhibits single-exponential behavior at T_f and that nonexponential kinetics does not emerge until the temperature is much lower than T_f, whereas that on a highly frustrated landscape starts to deviate from exponential behavior at just below the collapse temperature T_c, where the kinetics is controlled by escape rates from different low-lying energy traps. From such distinctive kinetics, they postulated that good folding sequences must be associated with such a minimally frustrated landscape and must have a diffuse transition state in order to be robust against variations in the protein environment and against mutations of the sequence.

For two-basin dynamics (i.e., chemical reactions), both theoretical[11−15] and experimental[16,17] developments in the past

† Part of the special issue "R. Stephen Berry Festschrift".

* Corresponding author. E-mail: tamiki@kobe-u.ac.jp. Phone: 81-78-803-5739. Fax: 81-78-803-5757.

‡ Kobe University.

§ The University of Chicago.

10.1021/jp025773j CCC: $22.00
Published on Web 08/31/2002

decades have shed light on the mechanics of passage through the saddles in the potential energy surfaces. Berry and coworkers[11−15] have analyzed local Liapunov functions and Kolmogorov entropies of several atomic clusters with three to seven atoms and have revealed that near the threshold energies at which the system can just cross the saddle trajectories passing through the saddle become collimated and more regularized, posing approximate local invariants of motion, than trajectories in the potential well in which the dynamics is fully chaotic. Recently, Komatsuzaki and Berry[18−23] clarified that irrespective of the system, even at higher energies above the threshold where mode−mode mixing wipes out most invariants of motion, one can, nonetheless, extract a ballistic reaction coordinate that rotates away almost all recrossings to single crossings in the region of first-rank saddles. Many nonstochastic, dynamical transitions have also been reported in simulation studies on phase transitions of small clusters,[24] the Lennard-Jones liquid,[25] and liquid water.[26] For example, the transitions among the inherent structures of liquid water occur intermittently not as simple diffusive motions of individual molecules but as cooperative dynamical processes with collective molecular motions.

The observed kinetics of protein folding is a consequence of averaging over an ensemble of many activated barrier crossings with multiple time scales. The future of the recent remarkable experimental developments in single-molecule spectroscopy[27−29] holds great promise in revealing the complexity of protein dynamics. One of the stimulating subjects is, for example, If non-Brownian dynamics that is somehow inherent to the individual molecule exists, can it assist the robustness of protein folding[8] and/or functions[30] in addition to the design of the energy landscape that the protein might have acquired by mutations?

The purpose of the present article is to scrutinize how time series of scalar quantities can shed light on the complexity of protein dynamics by means of several nonlinear time-series analyses.[31−33] The analyses we use here have been originally developed in the field of nonlinear science to discriminate chaotic and stochastic dynamics and are, in principle, applicable to any time series of any observable. As an illustrative vehicle, we use an off-lattice 46-bead model[10,34−38] that folds into a β-barrel native structure. The topography of the potential energy landscape for this model has been well surveyed in terms of its disconnectivity graph.[36] We investigate the complex dynamics involving multibarrier crossings using constant-temperature MD simulation and analyze the time series of the projections of the Cartesian coordinates of each bead into the principal components[39−42] at several temperatures.

The remainder of this article is organized as follows. In section II, we describe our method and technique. In section III, we describe the model and the calculations. We present our results and discussion in section IV. Finally, we give some concluding remarks in section V.

II. Theory

What can we learn or deduce from an observed *scalar* time series about the *multivariate* state (or phase) space buried in the observations? The so-called embedding theorem[31] attributed to Takens[45] provides us with a clue to the answer of such a question. Suppose that we have a nonlinear dynamical system (i.e., first-order d-dimensional ordinary differential equations)

$$\frac{d\mathbf{x}(t)}{dt} = \mathbf{F}(\mathbf{x}(t)) \tag{1}$$

where $\mathbf{x}(t)$ and $\mathbf{F}$ are the d-dimensional vector representations of the state space variables ($x_1(t)$, $x_2(t)$,..., $x_d(t)$) and the one-to-one map ($\mathbf{F}_1$, $\mathbf{F}_2$,..., $\mathbf{F}_d$), respectively. It is supposed that all degrees of freedom more or less influence one another through explicit or implicit couplings and that the d-dimensional manifold is compact and smooth in the state space $\mathbf{x}$. Let there exist a scalar quantity $s(t)$ with infinitesimal precision, and suppose that $s(t)$ is derived by a smooth transformation h from $\mathbf{x}(t)$ (i.e., $s(t) = h(\mathbf{x}(t))$. The embedding theorem states that, in principle, from the knowledge of the infinite time series $s(t)$ an equivalent state space $\mathbf{y}(t)$ can be reconstructed that preserves the differential properties of the state space of the original multivariate variables $\mathbf{x}(t)$. A time-delay coordinate system $\mathbf{y}_d(n)$,

$$\boldsymbol{y}_d(n) = (s(n), s(n+\tau),\cdots, s(n+(d-1)\tau)) \tag{2}$$

has been often used to reconstruct the state space, where the d-dimensional state-space variables $\mathbf{y}_d(n)$ are represented in a discrete form with a time interval τ without loss of generality. How can one find the unknown dimension d from the time series of $s(n)$? If there actually exists a dynamical system behind the observation of $s(t)$, any orbit $\mathbf{y}$ should never cross with itself in the state space because of the uniqueness of the solution. (Remember that there exists no self-intersection in the phase space of Hamiltonian systems.) If a smaller dimension to reconstruct the state space is used, the orbit $\mathbf{y}$ will have self-intersections and cannot be "unfolded" because of the insufficient size of the chosen dimensionality. In other words, if a minimum dimension to unfold the orbit in the time-delay coordinate system is reached, this implies that a state space $\mathbf{y}$ equivalent to the original $\mathbf{x}$ can be reconstructed in such a sense that it has the same differential properties of the original manifolds. The embedding theorem holds irrespective of the choice of the delay time τ, but, in practice, the observed time series are always contaminated by noise, computer round-off errors, or a finite resolution of observations and are sampled up to a certain finite time. In this regard, the dimension, referred as the minimum embedding dimension d_L hereafter, reached for the reconstructed space $\mathbf{y}$ is not necessarily equal to the dimension d of the original state space of $\mathbf{x}$. The choice of delay time τ and the determination of the minimum embedding dimension d_L have been the central subjects in applying this method to any realistic time series. For example, to elucidate the Liapunov exponent and spectra from an experimental observation first requires us to reconstruct the state space from the scalar time series[32,33,46].

A. Averaged False Nearest Neighbors. We chose Cao's algorithm[47,48] to determine the minimum embedding dimension d_L for a given (finite) scalar time series $s(t)$ and a given delay time τ. This algorithm is based on the concept of "false nearest neighbors (FNN)".[49] According to Takens' theorem, if the correct minimum embedding dimension d_L is chosen, then the nearest-neighbor point of an arbitrary point along an orbit in state space $\mathbf{y}$ exists only because of the topological properties of the underlying manifold. However, if the chosen dimension is smaller than d_L, nearest neighbors in the reconstructed space are located because of the "false" projections onto a wrong dimensionality. These false nearest neighbors are eliminated as the dimension increases. To diagnose the convergence of the dimensionality needed to eliminate the FNN and find the minimum embedding dimension, Cao proposed the following practical scheme: let $\boldsymbol{y}_d(n(i, d))$ be the nearest neighbor of a point $\boldsymbol{y}_d(i)$ in the d-dimensional reconstructed space (here, d is designated as a tentative dimension) and define the quantity

$$a(i, d) = \frac{||\mathbf{y}_{d+1}(i) - \mathbf{y}_{d+1}(n(i, d))||}{||\mathbf{y}_d(i) - \mathbf{y}_d(n(i, d))||} \quad (3)$$

($i = 1, 2,..., N - \tau d$) where $||\cdot||$ is a measure of the Euclidean distance (e.g., the maximum norm). In this paper, we employed the Euclidean norm

$$||\mathbf{y}_d(k) - \mathbf{y}_d(l)|| = (\sum_{j=0}^{d-1}[s(k + j\tau) - s(l + j\tau)]^2)^{1/2} \quad (4)$$

$a(i, d)$ describes how the ith point along the orbit in the d-dimensional reconstructed space moves away from its nearest neighbor when the tentative dimension increases by 1. To diagnose the convergence of the dimensionality required to "unfold" the whole orbit $\mathbf{y}(t)$, one can follow how an indicator $E1$ changes as d increases. $E1$ is defined by the ratio of the mean value of all $a(i, d)$ values on the d-dimensional and $(d + 1)$-dimensional spaces:

$$E1(d) = \frac{E(d + 1)}{E(d)} \quad (5)$$

where

$$E(d) = \frac{1}{N - \tau d} \sum_{i=1}^{N - \tau d} a(i, d) \quad (6)$$

When $E1(d)$ converges to unity for d larger than a certain value d_0, one can choose $d_0 + 1$ as the minimum embedding dimension d_L. Because of finite sampling, the *exact* self-intersections in a reconstructed space $\mathbf{y}$ with too small a dimension would suddenly disappear when the dimension is increased. $E1$ can be regarded as a diagnosis to deduce the minimum embedding dimension from a given *finite* scalar time series.

All realistic finite time series of interest are contaminated by noise, round-off errors, and so forth. Moreover, both stochastic and high-dimensional chaotic time series may result in convergence of $E1(d)$ at a certain high dimension d, and it is very difficult to identify the origin of this convergence, that is, whether the convergence arises from a high-dimensional chaos or from a stochastic but finite time series. To discriminate stochastic time series from high-dimensional chaos, Cao proposed[47,48] a supplemental diagnosis $E2$ defined by

$$E2(d) = \frac{E^*(d + 1)}{E^*(d)} \quad (7)$$

where

$$E^*(d) = \frac{1}{N - \tau d} \sum_{i=1}^{N - \tau d} |s(i + \tau d) - s(n(i, d) + \tau d)| \quad (8)$$

$E^*(d)$ is relevant to how the nearest neighbors will, on average, move away from one another in a finite time τd in the reconstructed space of a chosen dimension d. If the time series $s(n)$ is driven by a stochastic system, the progress in time of the variable should be almost independent of the previous value, and one can expect $E^*(d)$ to be almost constant irrespective of the choice of d. Thus, the indicator $E2$ will be approximately unity, independently of d. However, if $s(n)$ arises from a dynamical system, $s(n)$ is expected to give rise to a large $E^*(d)$ at small values of d ($\ll d_L$) because of the existence of false nearest neighbors, resulting in a significant dependence of $E2$ on d for certain low values of d where FNN still exist. As d increases, $E^*(d)$ will also increase because of a larger separation τd, but after reaching the minimum embedding dimension (i.e., one that preserves the topological features of its original manifold), E^* is expected to be unaffected by the change $d \rightarrow d + 1$, resulting in the convergence of $E2$ to approximately unity.

B. Average Mutual Information. Takens' theorem implies that the embedding dimension estimated by using time-delay coordinates should be independent of the value of τ. In practice, it depends on the value of τ because of unavoidable finite precision (e.g., computer round-off errors) and the finite length of the time series. This requires us to choose an appropriate time delay τ for every observable s: if τ is much shorter than a characteristic time scale inherent to the system in question, the successive points $\mathbf{y}(n)$, $\mathbf{y}(n + \tau)$, $\mathbf{y}(n + 2\tau)$... in the delay-time space will "collapse" onto a diagonal "region" $\mathbf{y}(n) \simeq \mathbf{y}(n + \tau) \simeq \mathbf{y}(n + 2\tau)$..., inside of which it might be impossible or very hard to distinguish the points from one another because of the limited, finite resolution of $s(n)$. That is, too short of a τ means that the system cannot move about the state space enough to produce, in practice, new information about the geometric features of the state space. However, if τ is too large, then the successive points may become numerically tantamount to being "random," even if $s(n)$ originally arises from a deterministic system with a finite dimensionality. That is, because of the orbital instability inherent to chaotic systems, when $\tau \rightarrow$ very large values, one cannot obtain the precision required to extract the deterministic structure buried in the random time series and to prevent exponential divergence.

Here, we chose a prescription[50] based on the concept of average mutual information in information theory. The average mutual information I_{AB} between measurements A and B is defined by

$$I_{AB} \equiv \sum_{a,b} P_{AB}(a, b)\, I_{AB}(a, b) \quad (9)$$

$$= \sum_{a,b} P_{AB}(a, b) \log_2\left[\frac{P_{AB}(a, b)}{P_A(a)\, P_B(b)}\right] \quad (10)$$

where $P_{AB}(a, b)$ is the joint probability density that a and b will be observed in measurements A and B, respectively, and $P_A(a)$ and $P_B(b)$ are the corresponding individual probability densities. $I_{AB}(a, b)$ represents the amount learned by the observation of a in measurement A about b in measurement B (and vice versa) in bits. If these two observations from measurements A and B are completely independent (i.e., if $P_{AB}(a, b) = P_A(a)\, P_B(b)$), $I_{AB}(a, b) = 0$. The average mutual information I_{AB}, an average of $I_{AB}(a, b)$ over all observations {a} and {b}, thus implies the degree of mutual correlation of the two measurements A and B. Fraser and Swinney[50] used an average mutual information, $I(t)$ with the value of $s(n)$ as the set of measurement A and the value of $s(n + t)$ as that of measurement B,

$$I(t) = \sum P(s(n), s(n + t)) \log_2\left[\frac{P(s(n), s(n + t))}{P(s(n))\, P(s(n + t))}\right] \quad (11)$$

They proposed to take the time $t_{min}(\equiv \tau)$ of the first minimum of $I(t)$ as a characteristic time scale inherent to the system. It is known[32,33] empirically that this simple prescription using $I(t)$ provides a good delay time τ for practical purposes and works better than using the linear autocorrelation function $\langle(s(n) - \bar{s})(s(n + t) - \bar{s})\rangle$ ($\bar{s}$ is the time average of s).

C. Principal Component Analysis. There is no general answer of what kinds of observable(s), coordinate(s), or projection(s) is(are) best to reveal the mechanism of complexity of nonlinear dynamics of multidimensional chaotic systems (e.g., proteins and biological systems). We chose in this report the so-called principal component (PC) analysis[39−42] to determine a set of linear, collective coordinates to best represent the most fluctuations of the system. Suppose we have n data points associated with p variables (e.g., n instantaneous structures of $3N$ Cartesian coordinates of N particles along an MD trajectory). Let **D** be an $n \times p$ matrix whose elements d_{im} are defined as the deviation of the (mass-weighted) ith Cartesian coordinate $X_i(t_m)$ at a time t_m ($1 \le m \le n$) from the time average $\langle X_i \rangle$:

$$d_{im} = X_i(t_m) - \langle X_i \rangle \tag{12}$$

where

$$\langle X_i \rangle = \frac{1}{n}\sum_{m=1}^{n} X_i(t_m) \tag{13}$$

Then, using a $p \times p$ variance−covariance matrix **R**,

$$\mathbf{R} = \frac{1}{n}\mathbf{D}\mathbf{D}^{\mathrm{T}} \tag{14}$$

(where $\mathbf{D}^{\mathrm{T}}$ is the transpose matrix of ***D***), whose second-moment element r_{ij} is

$$r_{ij} = \frac{1}{n}\sum_{m=1}^{n} (X_i(t_m) - \langle X_i \rangle)(X_j(t_m) - \langle X_j \rangle) \tag{15}$$

we can define a set of principal components **Q** by using the eigenvectors **U** that diagonalize **R**:

$$\mathbf{RU} = \mathbf{Ur}(\mathbf{U}^{\mathrm{T}}\mathbf{U} = \mathbf{I}) \tag{16}$$

The eigenvalue r_i, the ith element of the diagonal matrix **r**, represents the variance of the ith collective coordinate Q_i:

$$Q_i = \sum_{j=1}^{p} u_{ji} X_j \tag{17}$$

The larger the r_i, the more Q_i represents the configurational protein fluctuations. Throughout this paper, the principal components **Q** are sorted in order of decreasing variance, $r_1 \ge r_2,..., \ge r_p$. Note that a complementary approach, the so-called principal coordinate analysis,[43] that replaces eq 14 by an $n \times n$ matrix, $\mathbf{R} = {}^1/_p\mathbf{D}^{\mathrm{T}}\mathbf{D}$, has also been studied by Becker and Karplus[44] and Elmaci and Berry[35] to visualize the complexity of the multidimensional energy landscapes of proteins.

III. Model And Calculations

In the present paper, we apply these analyses to time series over a wide range of temperatures of a coarse-grained, off-lattice, 3-color, 46-bead protein model.[34−36] The rigid bonds of the original model by Honeycutt and Thirumalai[37,38] are replaced with stiff but harmonic spring-like bonds. The model is composed of hydrophilic (L), hydrophobic (B), and neutral (N) beads interacting with the following potential:

$$V = \sum_{i}^{\text{bonds}} K_r(r_i - r_0^i)^2 + \sum_{i}^{\text{angles}} K_\theta(\theta_i - \theta_0^i)^2 + \sum_{i}^{\text{dihedral}} [A(1 + \cos\Phi_i) + B(1 + \cos 3\Phi_i)] + \sum_{i<(j-3)}^{\text{nonbonded pairs}} 4\epsilon S_1\left[\left(\frac{\sigma}{R_{ij}}\right)^{12} - S_2\left(\frac{\sigma}{R_{ij}}\right)^{6}\right]$$

In this potential, the van der Waals (vdW) interactions are used to mimic the hydrophilic, hydrophobic, and neutral characters of the beads: $S_1 = S_2 = 1$ for BB (attractive) interactions, $S_1 = {}^2/_3$ and $S_2 = -1$ for LL and LB (repulsive) interactions, and $S_1 = 1$ and $S_2 = 0$ for the other sets involving N, expressing only excluded-volume interactions. For the bond-stretching and angle-bending force constants, we use $K_r = K_\theta = 20\epsilon(\mathrm{rad})^{-2}$, with the equilibrium bond length $r_0^i = \sigma$ and the equilibrium bond angle $\theta_0^i = 1.8326$ rad. Throughout this paper, the units of energy, temperature, bead mass, time, and frequency are ϵ, ϵ/k_{B}, M, $t^* = \sigma\sqrt{M/\epsilon}$, and $1/t^*$, unless otherwise noted. The sequence $B_9N_3(LB)_4N_3B_9N_3(LB)_5L$ folds into a lowest-energy β-barrel structure with four strands.[37,38] Folding into this structure is ensured by setting up the dihedral potential so that there are stiff trans preferences in the four strands, whereas at the loop regions consisting of neutral beads, the dihedral potential has a small barrier with no preference for any of the three rotameric states. In particular, $A = B = 1.2\epsilon$, except for dihedral angles involving two or more neutral residues where $A = 0$ and $B = 0.2\epsilon$. This model, referred to as BLN hereafter, exhibits highly frustrated potential energy topography[10,36] rather than ideal funnel-like topography. We examine both the original BLN model and a less-frustrated Gō-like BLN model studied by Nymeyer et al.[10] in which only 47 native contact pairs of hydrophobic beads possess attractive vdW interactions, whereas the interactions between all the other pairs are repulsive, which is responsible for the excluded volume. For the constant-temperature MD simulation, we used Berendsen's method[51] with a time step of $0.0025t^*$ in which the system is weakly coupled to an external heat bath with a coupling time of $5t^*$. This method does not involve any explicit stochastic variables in the equation of motion and can control the temperature well with minimal local disturbance to the system. Here, we focus on analyzing the internal conformational dynamics of the system and eliminate the total translational and rotational contributions.[52] The trajectory calculations are performed over a wide range of temperatures ranging from 0.2 to 5.0. The simulation at each temperature is preceded by a 10^5-step equilibration starting from the final conformation of the previous higher temperature. At each temperature, the trajectory data are collected every 100 steps for up to 10^7 steps($= 25\,000t^*$).

IV. Results and Discussion

In Figures 1 and 2, representative time series of potential energies $V(t)$ are shown at $T = 0.2$, 0.72, and 2.0 for the BLN model and at $T = 0.2$, 0.6, and 2.0 for the Gō-like model. As discussed by Nymeyer et al.,[10] the Gō-like model manifestly exhibits a two-state-like transition about the folding temperature, $T = 0.6$, because of its less-frustrated energy landscape. The potential energy fluctuation of the BLN model is rather diffuse, whereas one may expect the existence of "long-lived" memory in the time series about the collapse temperature, $T = 0.72$, when compared with that of the other temperatures.[53] Figures 3 and 4 show the so-called Allan variance[54−56] of the time series

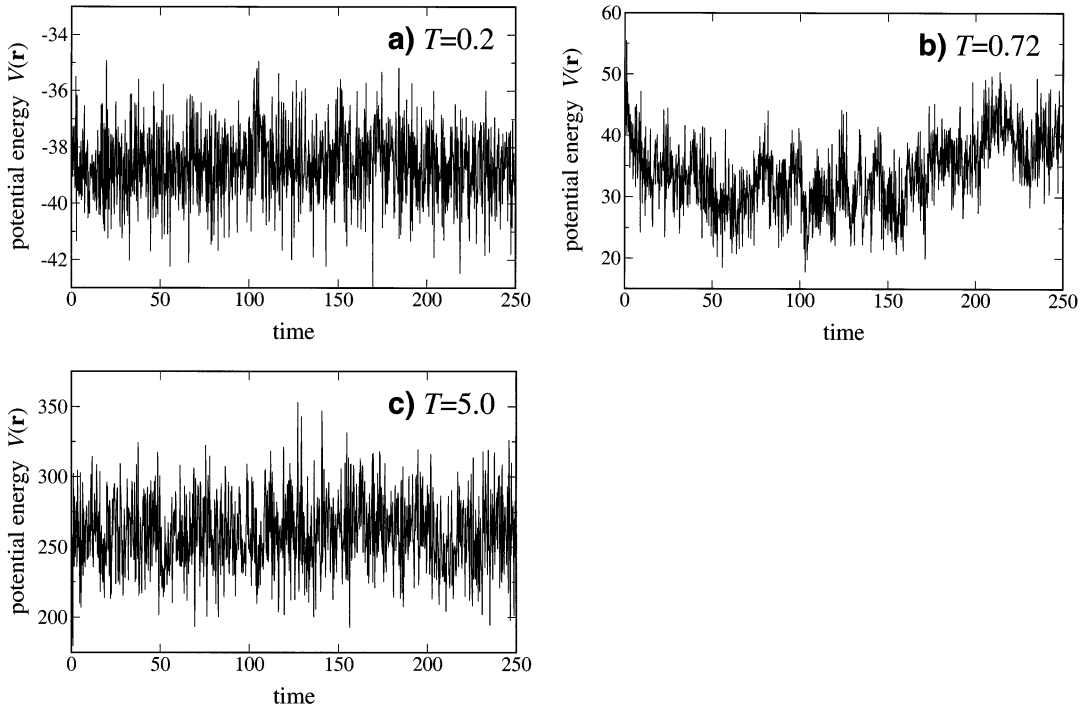

Figure 1. Potential energy fluctuations of the original BLN model. (a) $T = 0.2$, (b) $T = 0.72$, and (c) $T = 2.0$.

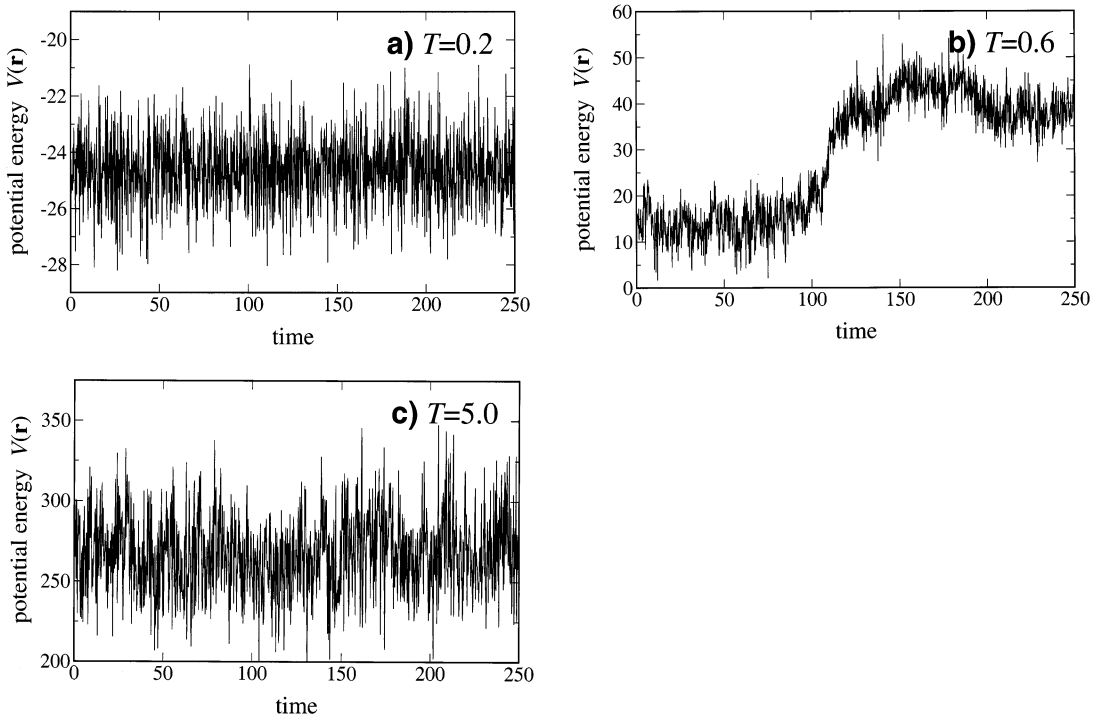

Figure 2. Potential energy fluctuations of the Gō-like BLN model. (a) $T = 0.2$, (b) $T = 0.6$, and (c) $T = 2.0$.

of the potential energies of these models at several temperatures. The Allan variance $\sigma_A^2(N)$ is defined by

$$\sigma_A^2(N) = \frac{1}{2}\left\langle\left(\frac{1}{N}\sum_{i=1}^{N} s(i) - \frac{1}{N}\sum_{i=1}^{N} s(i+N)\right)^2\right\rangle \qquad (18)$$

and measures the degree of nonstationarity of a given time series $s(t)$. If $s(t)$ is stationary, the following scaling relation

$$\sigma_A^2(N) \approx \mathcal{O}(N^{-\gamma}) \qquad (\gamma \text{ is a positive constant}) \qquad (19)$$

should be satisfied, obeying the law of large numbers, which guarantees the validity of the Wiener−Khinchin theorem. If $s(t)$ is nonstationary, $\gamma < 0$. These Figures demonstrate that, for both the BLN and Gō-like models, significant nonstationary features emerge about the collapse and folding temperatures in $V(t)$ but diminish as the system departs from these transition temperatures. The emergence of the nonstationary feature is more pronounced in the Gō-like model than in the BLN model. In both models at these transition temperatures, the simple scaling relation $\sigma_A^2(N) \approx N^{-\gamma}$ is obeyed for $0 \le t \le 10^{0.2}t^*(= 1.6t^* \simeq 10^3$ simulation steps), after which the index γ changes

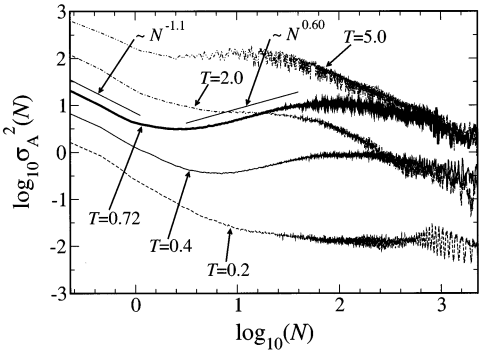

Figure 3. Allan variance of potential energy fluctuations of the original BLN model.

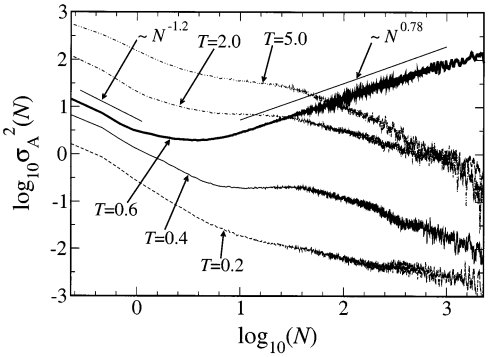

Figure 4. Allan variance of potential energy fluctuations of the Gō-like BLN model.

from positive (stationary regime: $\gamma \simeq -1.1$ (BLN), $\gamma \simeq -1.2$ (Gō-like)) to negative (nonstationary regime: $\gamma \simeq 0.60$ (BLN), $\gamma \simeq 0.78$ (Gō-like)). The nonstationary regime becomes stationary again near $100t^*$($\sim 10^5$ steps) for the BLN model, whereas it continues for even more than 10^5 steps for the Gō-like model (this strong nonstationary behavior for the Gō-like model was independent of the sampled trajectory, and only a few trajectories among the randomly sampled 100 trajectories exhibited the turnover from nonstationary to stationary regions at $\sim 100-1000t^*$, like those of the BLN model).

By using the Allan variance, Seko and Takatsuka[55] found in Ar_7 isomerization that a similar nonstationarity (i.e., $\gamma < 0$) also emerges at the transition temperature from solidlike to liquidlike phases, whereas the simple scaling relation $\sigma_A^2(N) \approx N^{-\gamma}$ ($\gamma > 0$) holds at the other temperatures. However, at the Ar_7 transition temperature, transitions between stationary and nonstationary regimes, such as those observed in both protein models, do not exist. This apparent distinction may arise from the generic feature inherent to the hierarchical energy landscapes in proteins. For short time scales, proteins move about only within an individual rugged basin and exhibit local stationary behavior due to the fast (chaotic) fluctuations. The longer the time, the more the protein crosses between large basins, bringing about large, slow fluctuations at the transition temperature. The longer persistence of the nonstationarity of the Gō-like model at T_f compared with that of the original BLN model may indicate that a less-frustrated funnel-energy landscape leads to longer memory persistence of the process at large.

Figure 5 depicts the power spectra $S(f)$ of the potential energy fluctuations of the original BLN and the Gō-like model at the collapse and folding temperatures, with

$$S(f) = \frac{1}{T}\left|\int_0^T \mathrm{d}t\, \mathrm{e}^{2\pi i f t} V(t)\right|^2 \qquad (20)$$

Both models exhibit a $1/f$ noise-like spectral density that can be expressed as $1/f^{\alpha}$, where $\alpha = 1.4$ for the BLN model and 1.5 for the Gō-like model. It is noteworthy that in the case of the Gō-like model this behavior persists over 3 decades of frequency, extending into the low-frequency regions, whereas for the BLN model, the $1/f$-like spectrum extends for only 2 decades, with the crossover to white noise occurring at higher frequencies. This supports the conclusions from the analysis of the Allan variance that the nonstationarity of the Gō-like model is enhanced at the transition temperature. Figure 6 presents α for both models as a function of temperature. The Gō-like model exhibits a much sharper transition to a white-noise spectrum than the BLN model as the temperature departs from the transition temperature. This finding also mirrors the results obtained from the Allan variance, in which the Gō-like model exhibits a sharp transition to nonstationarity around the transition temperature, whereas this transition is diffuse in the BLN model. The appearance of $1/f$ noise has been linked by many authors to the existence of multiple-relaxation processes or intermittency.[9,26,57−59] Marinari et al. show that $1/f$ noise also arises from a random walk on a random self-similar landscape.[60] However, Brownian motion on a simple double-well surface would give $1/f^2$ noise. To clarify the origin of the observed power spectra, we compare the MD simulations with overdamped Langevin dynamics simulations[61] of up to 50 ns using the same potentials. In this case, the nonstationary behaviors (i.e., $\sigma_A^2(N) \approx N^{-\gamma}$ ($\gamma < 0$) and $S(f) \approx 1/f^{\alpha}$ of the potential energy fluctuations) are not so pronounced with $\gamma \simeq -0.4$ (BLN) ≈ -0.2 (Gō-like) ($\gamma \simeq 0.2$ (BLN) ≈ 0.15 (Gō-like) for the stationary parts) at the transition temperatures and powers of $\alpha \approx 0.5-0.7$ at $T = 0.2-5.0$ for both models.[62] This indicates that the emergence of a $1/f$-type spectrum is not due to Brownian motion but that it has a different origin. One possible interpretation for the appearance of $\alpha > 1$ is the intermittent nature of the nonstationary dynamics observed in the Allan variance analysis. Intermittent dynamics yields $1/f^2$ spectra when the jump time is close to zero, but when the jumps have a finite duration, a smaller exponent of $\alpha < 2$ is expected.[26,58,59]

Let us now examine how the principal components (PCs) shed light on the multidimensional dynamics of proteins. Figure 7 shows the variance σ_i^2 of the PC Q_1, Q_2,..., Q_{12} series relative to the total variance of the protein fluctuation, which is defined as

$$\sigma_i^2 = \frac{r_i}{\sum_{k=1}^{3N} r_k} \times 100\% \qquad (21)$$

at several temperatures for both models (r_i (≥ 0) is the ith eigenvalue of the variance−covariance matrix **R**). It was found, for both models, that 90% of the total configurational fluctuations can be well represented in terms of about 10 principal components at each temperature. At $T \approx 0.2-0.4$, most of the system fluctuations are approximately localized on a few PCs for both models. As the temperature increases, the system fluctuations become more delocalized, spreading over a wider range of the PCs. Note, however, that the number of PCs required to represent the total configurational fluctuation of the systems is largest about the transition temperatures, $T = 0.72$ (BLN) and $T = 0.6$ (Gō-like).

Next, how long does memory persist in the principal components $Q(t)$, and what are the characteristic time scales

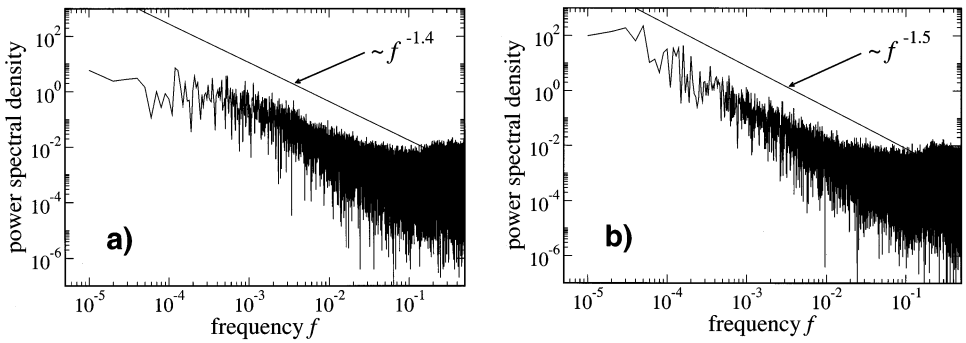

Figure 5. Power spectrum of potential energy fluctuations at transition temperatures. (a) Original BLN model and (b) Gō-like BLN model.

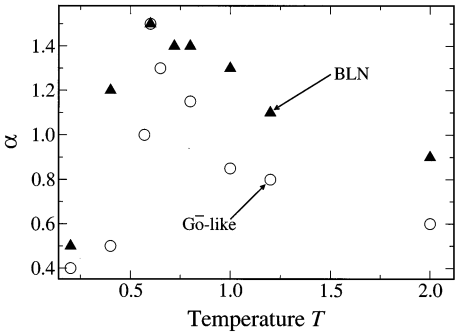

Figure 6. Power α of $1/f^{\alpha}$ as a function of temperature for the original BLN model and the Gō-like BLN model.

inherent to them? The average mutual information $I_i(t)$ of the individual principal component $Q_i(t)$ is one of the versatile means of measuring the degree of the mutual correlation of $Q_i(t_0)$ and $Q_i(t + t_0)$. Figure 8 depicts, as a representative example, $I_{10}(t)$ as a (logarithmic) function of time at $T = 0.2-5.0$ for the Gō-like BLN model. The times t_{min} of the first minimum of $I_{10}(t)$ are indicated by arrows. $I_{10}(t)$ has a longer tail in t at $T = 0.6$ than at the other temperatures, resulting in a longer t_{min}. Figure 9 shows the first minimum time t_{min} of each PC for both the BLN and Gō-like models at $T = 0.2-5.0$. In general, one can expect that the longer t_{min}, the longer the memory persistence in the signal $Q_i(t)$. Except for the PCs with very small variances, whose indexes are greater than ~100 for the BLN and ~80 for the Gō-like models, t_{min} values of almost all the other PCs exhibit a longer increase at the transition temperatures, $T = 0.72$ (BLN) and $T = 0.6$ (Gō-like), than do those at the other temperatures.

Now, let us try to look deeply into the question of what is the dimensionality of the state space, which is buried in the complexity of the time series of the protein dynamics. Here we apply Cao's embedding technique to every principal-component time series for the original BLN model over a wide range of temperatures. Figure 10 shows $E1(d)$ and $E2(d)$ of several principal components as a function of the tentative dimension d. In this Figure, (a), (b), and (c) display the principal components Q_1-Q_5, (d), (e), and (f) display $Q_{21}-Q_{25}$, and (g), (h), and (i) display $Q_{31}-Q_{35}$ at $T = 0.2$, 0.72, and 5.0, respectively. The more the variance (eigenvalue of the matrix **R**) of the PC decreases (i.e., the more the index of the PC increases), the more $E2(d)$ flattens to unity, resulting in a random time series with an "infinite" dimensionality. This implies that even if one reaches a finite dimensionality in terms of the $E1(d)$ such dimensionality should artificially arise from the finiteness of the sampling length. An observation from the embedding analysis that is perhaps even more striking appears in the behavior at the collapse temperature. That is, compared with the other temperatures, the model protein more likely preserves nonrandom characteristics for a wider range of principal components (i.e., the flattening of $E2(d)$ is more suppressed). Figures 11 and 12 show, respectively, the minimum of $E2(d)$, $E2_{min}$, and the minimum embedding dimension d_L of each principal component at several temperatures. Here, d_L is determined by the convergence of $E1(d)$ to within 95% of unity. $E2_{min}$ (= min{$E2(1)$, $E(2)$,..., $E2(d)$}) may indicate the degree of nonrandomness of the time series; as $E2_{min}$ goes to 1, $E2(d)$ becomes flatter independently of d. Figure 11 shows that as the temperature departs from the collapse temperature the $E2_{min}$ values of all the PCs approach unity. The smaller the variances of the PCs (i.e., as the index of the PCs increases), the faster the $E2_{min}$ values converge. Figure 12 confirms the conclusions from Figure 11: the larger the variance of the PC, the lower the dimensionality necessary to reconstruct the state space, and away from the collapse temperature, the dimensionality of the state space increases.

What is the implication of the dimension d_L evaluated by a scalar *finite* time series of each principal component of the *same* system? In Takens' theorem, the embedding dimension d is a global dimension equal to the number of (time delay) coordi-

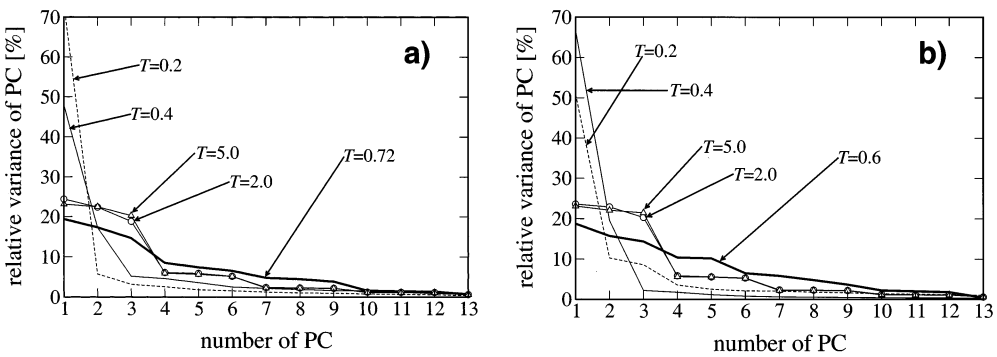

Figure 7. Relative variance σ_i^2 of the principal components Q_1, Q_2,..., Q_{12}. (a) Original BLN model and (b) Gō-like BLN model.

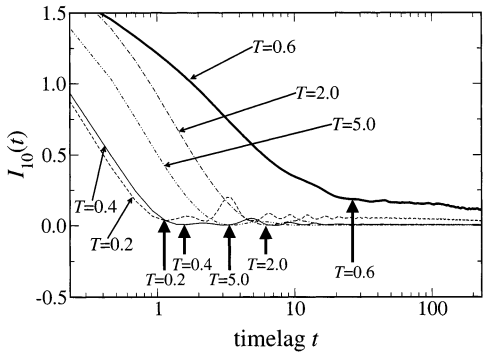

Figure 8. Average mutual information of the principal component $Q_{10}(t)$, $I_{10}(t)$, for the Gō-like BLN model at $T = 0.2-5.0$. The horizontal axis represents the log t, along which each arrow indicates the time of the first minimum of $I_{10}(t)$ at each temperature.

nates necessary to unfold an arbitrary orbit $\mathbf{y}_d(t)$ from self-intersections arising from a "wrong" projection to a lower-dimensional space. If one measures several observables or quantities from the same system to find the embedding dimension d, each measurement along with its time lags provides a different nonlinear mapping of the original state-space variables $\mathbf{x}(t)$ into a d-dimensional reconstructed space. Each should, in principle, reach the same global dimension inherent to the underlying dynamical structure under certain conditions (e.g., an infinite sampling length and an infinitesimal resolution). For a finite time evolution, however, each measurement may see different local topographies of the reconstructed state space and result in a different *local* dimensionality ($d_L \leq d$).

In principle, the time series of the principal components analyzed in this article should not be random because all the time series originally arise from the deterministic equation of motion. In this report, at each temperature for both of the models, we analyzed the time series collected every 100 simulation steps for up to 10^7 steps, that is, we could access the time series $Q(t)$ not with an infinitesimal resolution but with only a finite resolution.

The flattening observed in $E2(d)$ and the decreases of t_{min} for some principal components with small variances that are enhanced when departing from the transition temperature indicate that the fast chaotic fluctuations of the principal components cause the $Q(t)$ to "lose" their memory of the process quickly, resulting in a random stochastic time series. One cannot extract the geometric information of the underlying dynamical structure from any observable composed of such "lost" degrees of freedom.

Note that the corresponding time series $Q(t)$ collected at every step exhibits a strong d-dependency of $E2(d)$ and yields a finite dimension at these temperatures. At temperatures much lower than $T = 0.2$, where the system can move about a single local minimum only, say $T = 0.01$, the system motion is well represented by normal modes (i.e., fully regular dynamics), all the $E2(d)$ exhibit strong d-dependencies, and both the $E1(d)$ and $E2(d)$ quickly converge to unity at a small dimension, irrespective of the time period used to record the time series.

Almost all realistic observables of interest are always contaminated by noise and computer round-off errors with a finite resolution of observations and are sampled up to a certain finite time. It is not useful to inquire into the absolute value of the embedding dimension d_L from a given finite time series, especially for high-dimensional systems. However, an analysis of the dependence of d_L on, say, temperature, the choice of coordinates, projections, or observables can shed light on the dynamical structure of multidimensional complex systems. For high-dimensional systems of more than a few tens degrees of freedom, it might be impossible to attain sufficient sampling to find the nearest neighbors to a point $\mathbf{y}_d(n)$ besides the adjacent $\mathbf{y}_d(n+1)$ or $\mathbf{y}_d(n-1)$ points when d becomes very large, resulting in an apparent convergence at a certain high dimensionality, but still smaller than the desired high dimension. One plausible prescription might be to replace the searching of the nearest neighbors at every (recorded) step by searching at every 10 or more (recorded) steps.[63] Similarly, such a sampling problem arising from an insufficient search for the nearest neighbors that should converge to an adjacent point may also make it difficult to interpret the difference of d_L of several measurements from the same system. That is, different delay times τ of different measurements from the same system effectively yield different sampling lengths, which may result in an apparent difference of d_L arising not from the different local dimensionality of the dynamical structure but rather from the difference of sampling insufficiency. We examined the minimum embedding dimension d_L of each principal component with a delay time τ at each temperature whose sampling length N_{samp} was rescaled so as to be approximately equal to the minimum sampling length of $Q_1(t)$ at the transition temperature T_c with the maximum delay time τ_{max}:

$$N_{samp} \simeq \frac{\tau}{\tau_{max}} \times 10^5 \tag{22}$$

The results using the rescaled sampling length are qualitatively similar to the original ones, that is, the larger the variance of the PC, the lower the dimensionality, and away from the collapse temperature, the dimensionality of the PC increases. Here, the average numbers of nearest neighbors (besides adjacent points) of each principal component measurement are likely to be equal

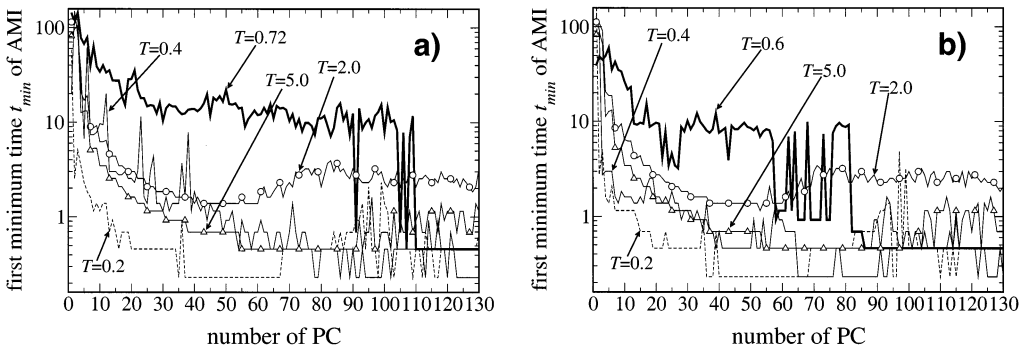

Figure 9. First minimum time τ of the average mutual information of all principal components. (a) Original BLN model and (b) Gō-like BLN model.

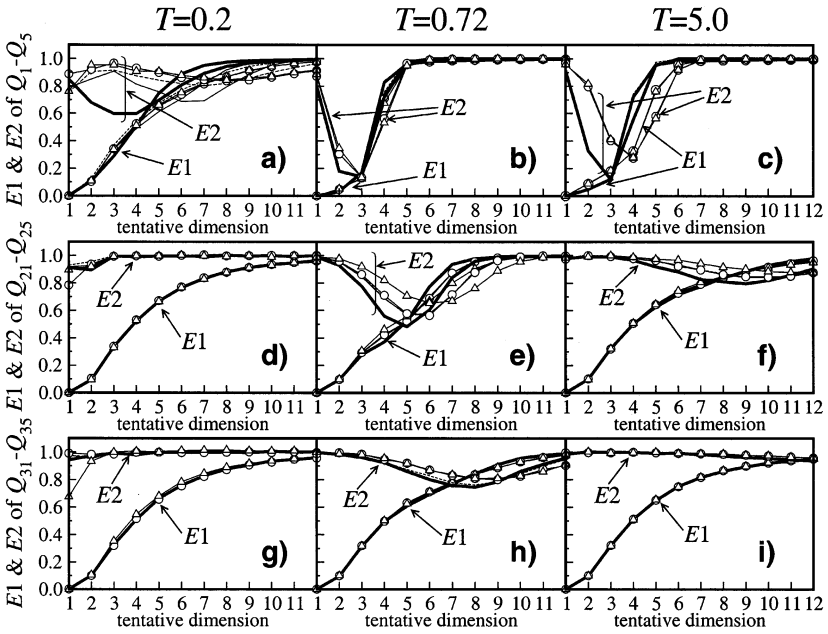

Figure 10. $E1(d)$ and $E2(d)$ of several principal components as a function of the tentative dimension d at $T = 0.2$, 0.72, and 5.0 for the original BLN model. (a) Q_1-Q_5 at $T = 0.2$, (b) Q_1-Q_5 at $T = 0.72$, (c) Q_1-Q_5 at $T = 5.0$, (d) $Q_{21}-Q_{25}$ at $T = 0.2$; (e) $Q_{21}-Q_{25}$ at $T = 0.72$, (f) $Q_{21}-Q_{25}$ at $T = 5.0$, (g) $Q_{31}-Q_{35}$ at $T = 0.2$, (h) $Q_{31}-Q_{35}$ at $T = 0.72$, and (i) $Q_{31}-Q_{35}$ at $T = 5.0$.

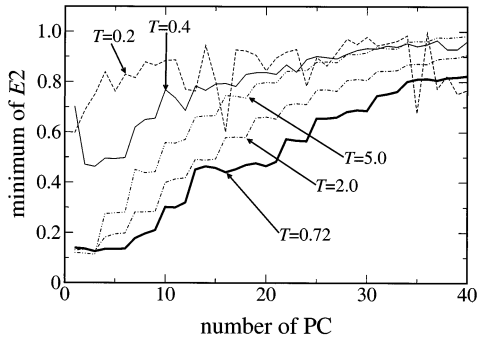

Figure 11. Minimum embedding dimension d_L estimated by the principal components at $T = 0.2$, 0.72, and 5.0 for the original BLN model.

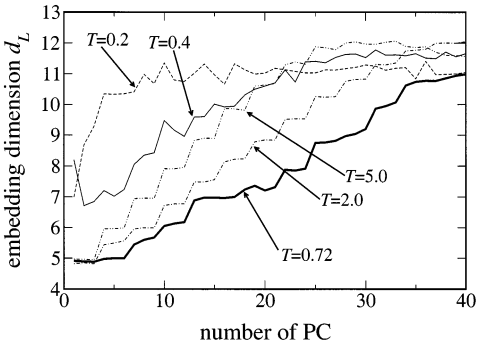

Figure 12. Minimum value of $E2(d)$ of the principal components at $T = 0.2$, 0.72, and 5.0 for the original BLN model.

to one other at all temperatures, except that at T_c they are relatively lower than at the other temperatures. This indicates that the observed distinctions in d_L at different temperatures may reflect differences in the local dimensionality of the state space structures and differences in some nonstationary features of the finite time series (i.e., the nonstationarity at the collapse transition temperature might require a longer time in comparison with the other temperatures to obtain reliable sampling of the nearest neighbors). Additional analysis is needed to inquire further into the problem.

V. Concluding Remarks

The law of kinetics describes the average behavior of populations of a state. The direct observation[27−29] of dynamical behavior of a single molecule, buried deeply in an ensemble average, should provide us with a new magnifying glass that enables us to "see" the dynamical structure of complex systems.[64] The nonlinear time-series analysis is one of the means to address this problem. In this article, we analyzed time series of potential energy fluctuations and principal components at several temperatures for two kinds of 46-bead models having two distinctive energy landscapes. The less-frustrated funnel-energy landscape (Gō-like BLN model) brings about stronger nonstationary behavior with the significant emergence of $1/f$ noise structure at the folding temperature than the other, rather frustrated energy landscape (original BLN model) at the collapse temperature. We also employed Cao's embedding analysis using the principal components of the original BLN model. The fast fluctuations with small amplitudes make the time series of ∼70−80% of the principal components almost random in only 100 simulation steps. It was found that the closer the temperature is to the collapse temperature, the more the stochastic feature of the principal components is suppressed through a wider range of degrees of freedom.

Principal component analysis (PCA) is one of the versatile means used to address the question of which coordinate(s) or projection(s) is(are) best to trace the underlying mechanism of dynamics in multidimensional complex systems. To what extent can the PCA actually mimic the dynamical behaviors of a set of original variables in terms of a reduced set of the new variables? The answer may depend on the degree of closeness of the distribution of the original data set to a Gaussian distribution. If the protein moves about only within a single basin, PCA is expected to work quite well[41,42] in describing multidimensional dynamical behaviors by using a reduced small set of the PCs (e.g., at $T = 0.2$ in Figure 7a and b). As the temperature increases above the transition temperature, the protein may find one or more reaction paths from one large basin to another and the transitions may take place through the curved or winding path(s). It is difficult for the standard PCA

algorithm to represent a curved or winding distribution in a reduced small set of the PCs, even while the PCA could still draw a rough sketch of the basin-to-basin transitions.

In this article, we scrutinized the dimensionality of the state space by using univariate time series (e.g., principal components) of the original BLN model. However, the development of time series analysis to multivariate observables[31,65] (e.g., embedding analysis using input−output data[48,63]) is desired in order to extract a good projection, thus revealing the dynamical structure from a limited set of observables. It is known[66,67] that the application of embedding analysis to time series involving intermittency, like those of the Gō-like model, is not straightforward and involves many problems that need to be overcome. The embedding analysis reconstructs the phase space in terms of the delay-time coordinate system, a complicated, abstract object of which one may not have a direct interpretation in terms of the phase-space variables. The Lie transform,[23] which transforms phase-space variables at any time $t + \tau$, $\mathbf{X}(t + \tau)$, into functions of $\mathbf{X}(t)$ at time t, can shed light on the implications of this abstract object, in principle, if the time evolution of $\mathbf{X}(t)$ arises from a Hamiltonian system. These are some of the subjects to be addressed in the future.

Acknowledgment. We dedicate this paper to Professor R. Stephen Berry and express our sincere gratitude for his continuous, warmest, stimulating guidance of our research. We thank Professors C.L. Brooks III, M. Sasai, A. Kitao, S. Takada, and M. Toda for their valuable discussions. T.K. thanks Professor Jack F. Douglas for pointing out García and Hummer's paper[6] and many relevant articles. This work was supported by the Japan Society for the Promotion of Science, Grant-in-Aid for Research on Priority Areas (A) "Molecular Physical Chemistry" and (C) "Genome Information Science" of the Ministry of Education, Science, Sports and Culture of Japan.

References and Notes

(1) Fersht, A. *Structure and Mechanism in Protein Science*; W. H. Freeman: New York, 1998.
(2) Karplus, M. *J. Phys. Chem. B* **2000**, *104*, 11.
(3) Gō, N. *Annu. Rev. Biophys. Bioeng.* **1983**, *12*, 183.
(4) Bryngelson, J. D.; Wolynes, P. G. *J. Phys. Chem.* **1989**, *93*, 6902.
(5) Takada, S. *Proc. Natl. Acad. Sci. U.S.A.* **1999**, *96*, 11698.
(6) García, A. E.; Hummer, G. *Proteins: Struct., Funct., Genet.* **1999**, *36*, 175.
(7) Shlesinger, M. F.; Zaslavsky, G. M.; Klafter, J. *Nature (London)* **1993**, *363*, 31. Shlesinger, M. F. Random Processes. In *Encyclopedia of Applied Physics*; Trigg, G. L., Ed.; VCH Publishers: New York, 1996; Vol. 16, p 45.
(8) Plotkin, S. S.; Wolynes, P. G. *Phys. Rev. Lett.* **1998**, *80*, 5015.
(9) Takano, M.; Takahashi, T.; Nagayama, K. *Phys. Rev. Lett.* **1998**, *80*, 5691.
(10) Nymeyer, H.; García, A. E.; Onuchic, J. N. *Proc. Natl. Acad. Sci. U.S.A.* **1998**, *95*, 5921.
(11) Amitrano, C.; Berry, R. S. *Phys. Rev. Lett.* **1992**, *68*, 729.
(12) Amitrano, C.; Berry, R. S. *Phys. Rev. E: Stat. Phys., Plasmas, Fluids, Relat. Interdiscip. Top.* **1993**, *47*, 3158.
(13) Hinde, R. J.; Berry, R. S. *J. Chem. Phys.* **1993**, *99*, 2942.
(14) Berry, R. S. *Chem. Rev.* **1993**, *93*, 2379.
(15) Berry, R. S. *Int. J. Quantum Chem.* **1996**, *58*, 657.
(16) Lovejoy, E. R.; Kim, S. K.; Moore, C. B. *Science (Washington, D.C.)* **1992**, *256*, 1541.
(17) Lovejoy, E. R.; Moore, C. B. *J. Chem. Phys.* **1993**, *98*, 7846.
(18) Komatsuzaki, T.; Berry, R. S. *J. Chem. Phys.* **1999**, *110*, 9160. Komatsuzaki, T.; Berry, R. S. *J. Chem. Phys.* **2002**, *116*, 862.
(19) Komatsuzaki, T.; Berry, R. S. *Phys. Chem. Chem. Phys.* **1999**, *1*, 1387.
(20) Komatsuzaki, T.; Berry, R. S. *J. Mol. Struct.: THEOCHEM* **2000**, *506*, 55.
(21) Komatsuzaki, T.; Berry, R. S. *Proc. Natl. Acad. Sci. U.S.A.* **2001**, *78*, 7666.
(22) Komatsuzaki, T.; Berry, R. S. *J. Chem. Phys.* **2001**, *115*, 4105.
(23) Komatsuzaki, T.; Berry, R. S. *Adv. Chem. Phys.* **2002**, *123*, 79.
(24) Nayak, S. K.; Jena, P.; Ball, K. D.; Berry, R. S. *J. Chem. Phys.* **1998**, *108*, 234.
(25) Donati, C.; Douglas, J. F.; Kob, W.; Plimpton, S. J.; Poole, P. H.; Glotzer, S. C. *Phys. Rev. Lett.* **1998**, *80*, 2338.
(26) Ohmine, I. *J. Phys. Chem.* **1995**, *99*, 6767.
(27) Yanagida, T.; Kitamura, K.; Tanaka, H.; Iwane, A. H.; Esaki, S. *Curr. Opin. Cell Biol.* **2000**, *12*, 20.
(28) Weiss, S. *Nat. Struct. Biol.* **2000**, *7*, 724.
(29) Ishii, Y.; Yoshida, T.; Funatsu, T.; Wazawa, T.; Yanagida, T. *Chem. Phys.* **1999**, *247*, 163.
(30) Wang, J.; Wolynes, P. G. *Phys. Rev. Lett.* **1994**, *74*, 4317.
(31) Sauer, T.; Yorke, J. A.; Casdagli, M. *J. Stat. Phys.* **1991**, *65*, 579.
(32) Abarbanel, H. D.-I. *Analysis of Observed Chaotic Data*; Springer-Verlag: New York, 1995.
(33) Kantz, H.; Schreiber, T. *Nonlinear Time Series Analysis*; Cambridge University Press: Cambridge, U.K., 1997.
(34) Berry, R. S.; Elmaci, N.; Rose, J. P.; Vekhter, B. *Proc. Natl. Acad. Sci. U.S.A.* **1997**, *94*, 9520.
(35) Elmaci, N.; Berry, R. S. *J. Chem. Phys.* **1999**, *110*, 10606.
(36) Wales, D. J.; Doye, J. P. K.; Miller, M. A.; Mortenson, P. N.; Walsh, T. R. *Adv. Chem. Phys.* **2000**, *115*, 1.
(37) Honeycutt, J. D.; Thirumalai, D. *Biopolymers* **1992**, *32*, 695.
(38) Guo, Z.; Brooks, C. L., III; Boczko, E. M. *Proc. Natl. Acad. Sci. U.S.A.* **1997**, *94*, 10161.
(39) *Computational Biochemistry and Biophysics*; Becker, O. M., MacKerell, A. D., Jr., Roux, B., Watanabe, M., Eds.; Marcel Dekker: New York, 2001.
(40) Levy, R. M.; Srinivasan, A. R.; Olson, W. K.; McCammon, J. A. *Biopolymers* **1984**, *23*, 1099.
(41) Kitao, A.; Hirata, F.; Gō, N. *Chem. Phys.* **1991**, *158*, 447.
(42) Kitao, A.; Gō, N. *Curr. Opin. Struct. Biol.* **1999**, *9*, 164.
(43) Gower, J. C. *Biometrika* **1966**, *53*, 325. Gower, J. C. *Biometrika* **1968**, *55*, 582.
(44) Becker, O. M.; Karplus, M. *J. Chem. Phys.* **1997**, *106*, 1495.
(45) Takens, F. Detecting Strange Attractors in Turbulence; In *Lecture Notes in Mathematics 898;* Springer: New York, 1981.
(46) Sano, M.; Sawada, Y. *Phys. Rev. Lett.* **1985**, *55*, 1082.
(47) Cao, L. *Physica D* **1997**, *110*, 43.
(48) Cao, L.; Mees, A.; Judd, K.; Froyland, G. *Int. J. Bifurcat. Chaos* **1998**, *8*, 1491.
(49) Kennel, M. B.; Brown, R.; Abarbanel, H. D.-I. *Phys. Rev. A: At., Mol., Opt. Phys.* **1992**, *45*, 3403.
(50) Fraser, A. M.; Swinney, H. L. *Phys. Rev. A: At., Mol., Opt. Phys* **1986**, *33*, 1134.
(51) Berendsen, H. J. C.; Postma, J. P. M.; van Gunsteren, W. F.; DiNola, A.; Haak, J. R. *J. Chem. Phys.* **1984**, *81*, 3684.
(52) For Berendsen's method, one could eliminate total translational and rotational contributions by setting to zero the total translational and angular momenta of the system. However, one may also see the complex issue of the so-called "falling cat" problem (Littlejohn, R. G.; Reinsch, M. *Rev. Mod. Phys.* **1997**, *69*, 213).
(53) For the sake of simplicity, we regard $T = 0.72$ as the "collapse" temperature of the BLN model and $T = 0.6$ as the "folding" temperature of the Gō-like model. This collapse temperature was that originally estimated for the original Honeycutt−Thirumalai rigid-bond force-field potential.[37] The folding temperature was chosen such that two-state-like transitions are often observed at the temperature of our simulation run. This temperature is a bit higher than that of the simulation by Nymeyer et al.,[10] which uses the original force-field potential.
(54) Allan, D. W. *Proc. IEEE* **1966**, *54*, 221.
(55) Seko, C.; Takatsuka, K. *J. Chem. Phys.* **1996**, *104*, 8613.
(56) Tanaka, K.; Aizawa, Y. *Prog. Theor. Phys.* **1993**, *90*, 547.
(57) Weissman, M. B. *Rev. Mod. Phys.* **1988**, *60*, 573.
(58) Aizawa, Y.; Kikuchi, Y.; Harayama, T.; Yamamoto, K.; Ota, M.; Tanaka, T. *Prog. Theor. Phys. Suppl.* **1989**, *36*, 985.
(59) Aizawa, Y. *Chaos, Solitons Fractals* **2000**, *11*, 263.
(60) Marinari, E. G.; Parisi, G.; Ruelle, D.; Windey, P. *Commun. Math. Phys.* **1982**, *89*, 1.
(61) van Gunsteren, W. F.; Berendsen, H. J. C. *Mol. Phys.* **1982**, *45*, 637.
(62) Kostov, K. S.; Matsunaga, Y.; Toda, M.; Komatsuzaki, T. Unpublished work.
(63) Walker, D. M.; Tufillaro, N. B. *Phys. Rev. E: Stat. Phys., Plasmas, Fluids, Relat. Interdiscip. Top.* **1999**, *60*, 4008.
(64) Metzler, R.; Klafter, J.; Jortner, J. *Proc. Natl. Acad. Sci. U.S.A.* **1999**, *96*, 11085.
(65) Cao, L.; Mees, A.; Judd, K. *Physica D* **1998**, *121*, 75.
(66) Platt, N.; Spiegel, E. A.; Tresser, C. *Phys. Rev. Lett.* **1993**, *70*, 279.
(67) von Hardenberg, J. G.; Paparella, F.; Platt, N.; Provenzale, A.; Spiegel, E. A.; Tresser, C. *Phys. Rev. E: Stat. Phys., Plasmas, Fluids, Relat. Interdiscip. Top.* **1997**, *55*, 58.